Manganese 3*d* and 4*s* Electron-density Distribution in Phthalocyaninato-manganese(II)

By **Brian N. Figgis, Edward S. Kucharski,** and **Geoffrey A. Williams,*** School of Chemistry, University of Western Australia, Nedlands, Western Australia 6009

A new analysis of the 116 K single-crystal *X*-ray diffraction data set of good accuracy on β-phthalocyaninato-manganese(II) has yielded individual 3*d* and 4*s* orbital populations on the manganese atom of significant accuracy and qualitative estimates of bonding electron density in the macrocycle ring. The manganese orbital populations (*x* and *y* along Mn–N vectors, *z* perpendicular to the square plane of co-ordinated nitrogen atoms) have been determined by a least-squares refinement procedure as $d_{xy}^{1.5(2)}$, $d_{xz}^{0.6(2)}$, $d_{yz}^{0.7(2)}$, $d_{z^2}^{0.9(2)}$, $d_{x^2-y^2}^{0.1(2)}$, and $4s^{2.0(3)}$. Difference-Fourier syntheses indicate the aspherical nature of the valence charge density on the manganese atom, and the presence of bonding charge density in the ligand. In the later stages of the structural and orbital population analyses, allowance was made in the scattering model for overlap charge density by placing small spherical charges of variable population and radial extent between C–C and C–N atom pairs and in the Mn–N vectors. The present treatment of the data differs from the previous analysis in that refinement of atomic positional and thermal parameters has been based upon intensities (I), and all 2 265 observations with $(\sin\theta)/\lambda \leqslant 0.662$ Å^{-1}, rather than on structure factor amplitudes ($|F|$) and only the 1 608 reflections with $I > 3\sigma(I)$. Full-matrix least-squares refinement on the basis of a spherical atom model yielded R 0.045, and bond lengths and angles of improved accuracy are reported. The atomic positional and thermal parameters thus obtained have been used to generate a set of ' difference structure factors,' F_d, containing, principally, information about the valence charge density on the manganese atom. These F_d values have been analysed by least-squares refinement in terms of aspherical density arising from 3*d* and 4*s* orbital populations on the manganese atom. The present analysis has established that worthwhile information on chemical bonding in a molecule as large as a transition-metal macrocycle can be obtained from a low-temperature *X*-ray data set of good quality, and acts as a guide for a program to involve the collection of low-temperature data sets of excellent quality for this purpose.

THE geometrical structures of the metallophthalocyanines have been studied extensively, in particular by single-crystal *X*-ray diffraction techniques (ref. 1 and refs. therein), largely on account of their generic relation to the naturally occurring porphyrins, chlorins, and corrins. We have initiated a program to study the chemical bonding in the metallophthalocyanines, using the techniques of *X*-ray and neutron diffraction over the temperature range 4.2 to 295 K [1-3] and polarised neutron diffraction at 4.2 K.[4] The former studies have been designed to determine accurately the molecular structures for use in conjunction with the polarised neutron program. We have used this information to deduce spin-density distributions in paramagnetic phthalocyaninato-manganese(II), [Mn(pc)], and -cobalt(II), [Co(pc)] (pc = phthalocyaninate).

It is an attractive proposition to complement these studies with the determination of valence-electron densities using accurate single-crystal diffraction data. Such electron-density studies have recently been made on several transition-metal compounds.[5] The experimental difficulties [6] inherent in every valence-electron density study using either extensive and accurate *X*-ray diffraction data alone, or combined with a neutron diffraction definition of nuclear positional and vibrational parameters, are compounded in the case of compounds containing a heavy atom such as a transition metal. This is because the valence-electron densities are very small in relation to the high electron density of the transition-metal core. That the asphericity of the charge about an open-shell transition metal, due to the *d* electrons, is quite small is evident from the very many successful molecular-structure determinations of transition-metal compounds using single-crystal *X*-ray diffraction data. In these determinations, which consistently yield low *R* factors for the agreement between observed and calculated structure factors, a spherically symmetrical metal-atom scatterer is used.

In preference to embarking on a full-scale valence-electron density study of [Mn(pc)] and [Co(pc)], in which a very considerable effort would be required to obtain the most accurate diffraction data possible, we have undertaken the present study using data for [Mn(pc)], already at hand, which is of good accuracy. The overall aim of this present study is to guide thorough investigations of the valence-electron density in metallo-organic and other compounds of this type, and to assess the value they are likely to have in understanding the chemical bonding. If such a study is likely to be successful, it is important to be able to optimise experimental conditions such as the choice of compound and crystal, the accuracy and extent of the *X*-ray diffraction data required, and the temperature. It is also of value to know whether an accurate *X*-ray diffraction data set alone can provide sufficient information without the need for support from neutron diffraction data. Finally, the present study was intended to investigate a novel method of analysing accurate *X*-ray data in a chemically meaningful way.

In a molecule such as a metallophthalocyanine, interest often focuses on the electronic structure of the metal atom, and we have concentrated upon this aspect. In [Mn(pc)], we have treated the ligand valence-electron distribution only as far as necessary to facilitate the determination of the manganese atom 3*d* and 4*s* electron distribution, including the extent of the delocalisation onto the ligand.

EXPERIMENTAL

The 116 K *X*-ray diffraction intensity data of a previous structural analysis of the β-polymorphic form of [Mn(pc)] [1] were used in the present work.

Crystal Data.[1]—$C_{32}H_{16}MnN_8$, $M = 567.49$, Monoclinic, space group $P2_1/c$, $a = 14.590(3)$, $b = 4.741(1)$, $c = 19.301(5)$ Å, $\beta = 120.79(1)°$, $U = 1\,146.9(4)$ Å^3, $Z = 2$, $D_c = 1.643$ g cm^{-3}, Mo-K_α radiation (graphite-crystal monochromator), $\lambda = 0.710\,69$ Å, $\mu = 6.530$ cm^{-1},[7] crystal dimensions $0.04 \times 0.10 \times 0.53$ mm, $T = 116 \pm 2$ K, 2 265 unique observations with $(\sin\theta)/\lambda \leqslant 0.662$ Å^{-1}.

Structure Refinement.—All 2 265 unique intensities measured [a complete sphere of data to $(\sin\theta)/\lambda \leqslant 0.595$ Å^{-1}, with the weakest reflections skipped for $0.595 < (\sin\theta)/\lambda \leqslant 0.662$ Å^{-1}] were corrected for absorption and included in the full-matrix least-squares refinement of atomic co-ordinates and thermal parameters. The program CRYLSQ [8] was used for least-squares refinement, the function minimised being $\Sigma w(\Delta I)^2$ where $\Delta I = I_o - I_c$ and $w = 1/\sigma(I)^2$ is the weight assigned to the I_o values. The refinement was based on I_o so that all measured data (including those observations with $I_o < 0$) could be included in the least-squares process, thereby eliminating the bias introduced into data by using a $\sigma(I)$ rejection criterion or by setting all negative intensities to zero.[9]

A total of 219 variables was refined in the least-squares refinement including all positional, anisotropic (C, N, Mn), and isotropic (H) thermal parameters. Refinement converged with $R(=\Sigma||\Delta I|/\Sigma|I_o|)$ 0.044, $R'\{=[\Sigma w(\Delta I)^2/\Sigma w I_o^2]^{\frac{1}{2}}\}$ 0.070, and $\chi\{=[\Sigma w(\Delta I)^2/(2\,265 - 219)]^{\frac{1}{2}}\}$ 1.484. The maximum shift-to-error ratio at convergence was 0.001 : 1. An examination of the final observed and calculated intensities revealed no evidence of any multiple scattering or secondary extinction effects and, in fact, in a trial least-squares cycle the extinction coefficient did not vary significantly from zero. On a final difference synthesis, the largest peaks were 0.81 at (000) and −0.68 e Å^{-3} at a position close to the Mn atom. Some difference-Fourier sections calculated through various planes at this stage (Level I) of the scattering model are shown in Figure 1.

Final atomic positional co-ordinates and thermal parameters, with estimated standard deviations in parentheses, are listed in Tables 1 and 2. Atomic scattering-factor curves for neutral Mn, C, and N were from ref. 10, and were modified for the real and imaginary anomalous dispersion corrections.[11] The scattering-factor curve for H was taken from ref. 12. Observed and calculated structure factors are listed in Supplementary Publication No. SUP 22755 (27 pp.).*

The aspherical deformation density around the Mn atom, obvious in the difference sections (Figure 1), provided the basic data for the following novel method for extracting valence orbital populations on transition metals in centrosymmetric cells. A 'difference structure factor', $F_d = F_o - F_c$, was calculated for each observation where F_c was obtained from the scattering model of the Level I stage of refinement, with the exception that for Mn the scattering curve for only the Ar core [13] was included in the calculation of F_c. That is, the spherical approximations to the C, H, and N atoms with their Level I positional and thermal parameters, together with the spherical Ar core of Mn^{2+}, were subtracted from the F_o, leaving a component, F_d, with contributions from the valence electrons of Mn together with aspherical valence density effects about the other atoms and experimental errors. A section of a Fourier synthesis using F_d as input is shown in Figure 2, and indicates the high degree to which a spherically symmetrical approximation to the Mn scatterer is valid. The method used to obtain phased, anomalous-dispersion-free F_o values for use in the calculation of F_d is presented in the Appendix.

The F_d values were then used in a least-squares refinement of a non-spherically symmetrical valence-electron model for Mn. For this purpose, the program ASRED written by two of us (G. A. W. and B. N. F.), was used. In ASRED a

* For details see Notices to Authors No. 7, *J.C.S. Dalton*, 1979, Index issue.

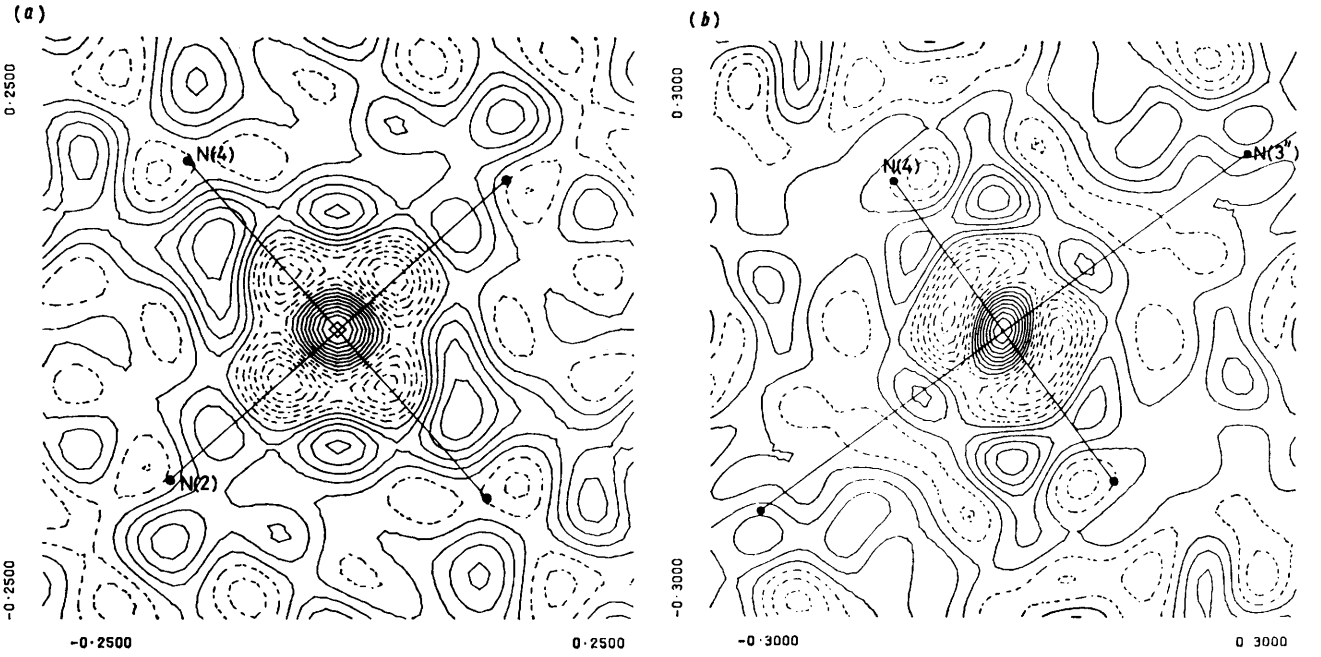

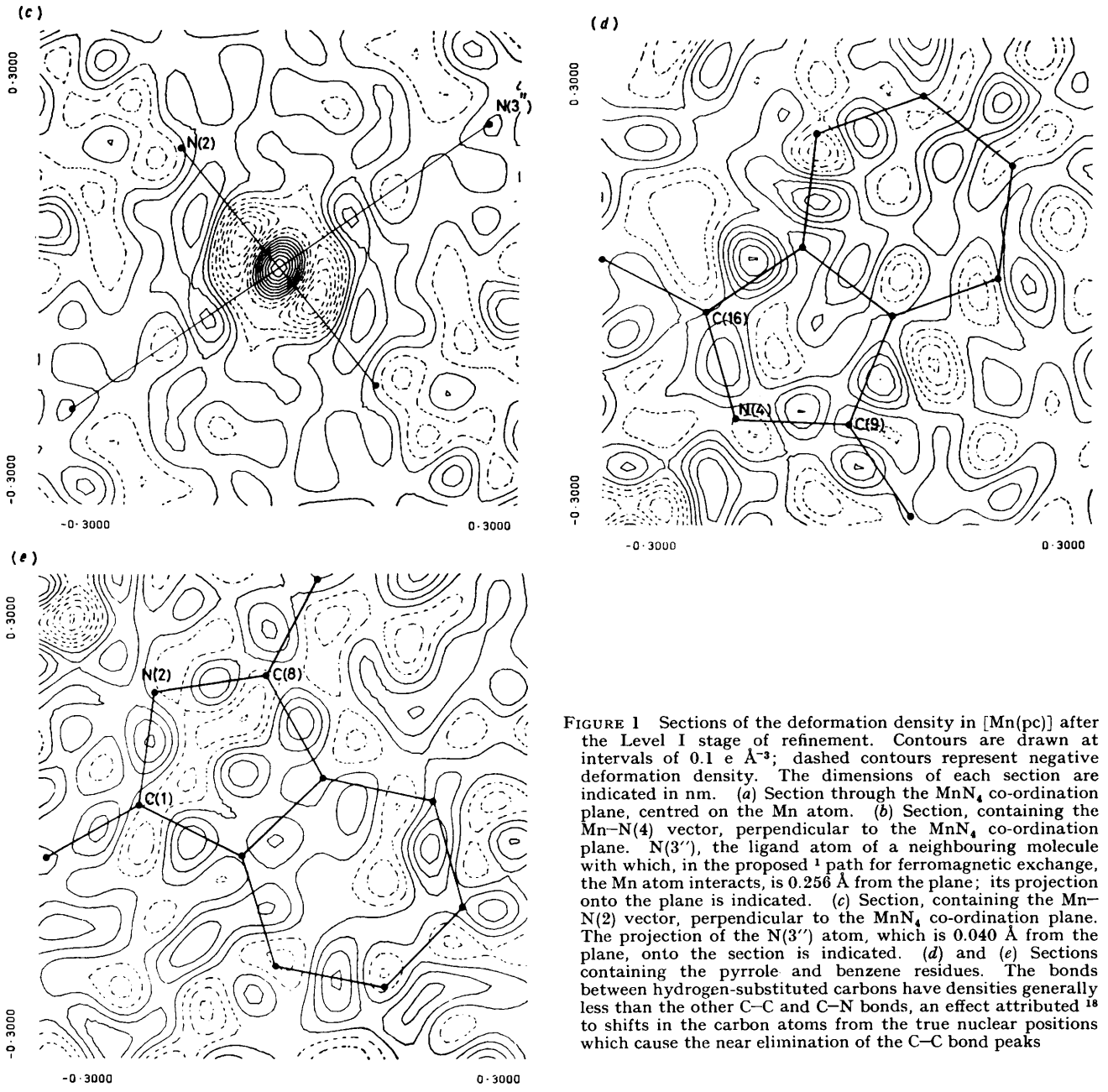

FIGURE 1 Sections of the deformation density in [Mn(pc)] after the Level I stage of refinement. Contours are drawn at intervals of 0.1 e Å^{-3}; dashed contours represent negative deformation density. The dimensions of each section are indicated in nm. (*a*) Section through the MnN_4 co-ordination plane, centred on the Mn atom. (*b*) Section, containing the Mn–N(4) vector, perpendicular to the MnN_4 co-ordination plane. N(3''), the ligand atom of a neighbouring molecule with which, in the proposed [1] path for ferromagnetic exchange, the Mn atom interacts, is 0.256 Å from the plane; its projection onto the plane is indicated. (*c*) Section, containing the Mn–N(2) vector, perpendicular to the MnN_4 co-ordination plane. The projection of the N(3'') atom, which is 0.040 Å from the plane, onto the section is indicated. (*d*) and (*e*) Sections containing the pyrrole and benzene residues. The bonds between hydrogen-substituted carbons have densities generally less than the other C–C and C–N bonds, an effect attributed [18] to shifts in the carbon atoms from the true nuclear positions which cause the near elimination of the C–C bond peaks

set of quantization axes is assigned to each atom, and the electronic valence populations of *s*, *p*, and *d* orbitals on each atom can be refined by a least-squares process, using the formalism of Weiss and Freeman.[14] Single-electron scattering curves $\langle j_0\rangle_{s,p,d}$, $\langle j_2\rangle_{p,d}$, and $\langle j_4\rangle_d$ for each atom type and each orbital type from a tabulated source,[13,15] or calculated from an atomic wave function,[16] are used in conjunction with the equations for the scattering by *p* [17] and *d* electrons.[14] Because such theoretical single-electron scattering curves apply to the free atom or ion, for atoms in a chemical environment it is necessary to allow some refinement of the scattering-curve shape. This is accomplished in ASRED by a least-squares refinement of an 'orbital-expansion' parameter *r* where f(*s*) [$=f_0(rs)$] is the single-electron scattering factor at $(\sin\theta)/\lambda = s$ and $f_0(rs)$ is the free-atom scattering factor at $(\sin\theta)/\lambda = rs$. The refinement of *r* is associated with variation of the radial exponents of the atomic wave function.

Only limited success was obtained in the refinement of an aspherical valence model for Mn using the F_d values described above. However, in the space group $P2_1/c$, a spherically symmetrical scatterer at (000) does not contribute to the class of reflections *hkl* with $k + l = 2n + 1$. Hence the Mn contribution to these reflections is extremely small, arising only from the aspherical components of both the valence electrons and the anisotropic thermal motion. Since most of this class of reflections has $|F_d|$ values of similar magnitude to the remaining reflections, to which Mn contributes strongly, it was apparent that aspherical valence density effects about the C and N atoms were the

major contributors to this $k + l = 2n + 1$ data. The valence-electron model for Mn was then refined using only 1 151 observations with $k + l = 2n$ and $(\sin\theta)/\lambda \leqslant 0.595$ Å^{-1}. The results are presented in Table 3. In the refinement, the function $\Sigma w(\Delta F_d)^2$ was minimized where $w = 1/\sigma(I)^2$ as before, and $\Delta F_d = |F_d - F_v|$ where F_v is the Mn valence-

TABLE 1

Final atomic positional co-ordinates for [Mn(pc)] at 116 K *

Atom	x/a	y/b	z/c
N(1)	0.252 8(1)	0.029 7(5)	0.161 2(1)
	0.253 4(1)	0.029 7(5)	0.161 5(1)
N(2)	0.073 1(1)	0.225 2(5)	0.097 2(1)
	0.073 4(1)	0.225 2(4)	0.097 4(1)
N(3)	−0.072 0(2)	0.530 4(5)	0.077 5(1)
	−0.072 1(1)	0.531 3(5)	0.077 7(1)
N(4)	−0.132 3(2)	0.199 6(5)	−0.033 5(1)
	−0.132 7(1)	0.199 8(4)	−0.033 7(1)
C(1)	0.180 2(2)	0.201 7(6)	0.158 8(1)
	0.179 8(2)	0.202 2(5)	0.158 7(1)
C(2)	0.200 7(2)	0.402 2(5)	0.222 0(1)
	0.200 7(2)	0.401 9(5)	0.222 0(1)
C(3)	0.291 6(2)	0.458 8(7)	0.296 8(2)
	0.292 4(2)	0.456 7(6)	0.296 9(1)
C(4)	0.283 1(2)	0.662 3(6)	0.344 1(2)
	0.283 7(2)	0.662 3(6)	0.344 7(1)
C(5)	0.188 0(2)	0.806 2(7)	0.319 2(2)
	0.187 9(2)	0.807 6(6)	0.319 6(1)
C(6)	0.097 9(2)	0.754 0(6)	0.245 2(2)
	0.097 0(2)	0.755 2(5)	0.245 0(1)
C(7)	0.105 8(2)	0.547 8(6)	0.197 1(1)
	0.105 7(2)	0.547 7(5)	0.197 0(1)
C(8)	0.027 7(2)	0.437 1(5)	0.119 1(1)
	0.027 8(2)	0.436 9(5)	0.119 1(1)
C(9)	−0.145 8(2)	0.416 0(5)	0.008 4(1)
	−0.145 6(2)	0.416 3(5)	0.008 5(1)
C(10)	−0.256 3(2)	0.503 6(7)	−0.033 1(1)
	−0.256 1(2)	0.503 3(6)	−0.033 0(1)
C(11)	−0.309 7(2)	0.702 5(6)	−0.014 3(2)
	−0.309 5(2)	0.704 7(5)	−0.013 7(1)
C(12)	−0.418 9(2)	0.731 3(7)	−0.067 3(2)
	−0.419 1(2)	0.733 1(6)	−0.067 2(1)
C(13)	−0.471 9(2)	0.568 0(6)	−0.136 6(2)
	−0.472 7(2)	0.568 4(5)	−0.137 1(1)
C(14)	−0.418 8(2)	0.369 7(6)	−0.155 7(2)
	−0.419 3(2)	0.368 4(5)	−0.156 2(1)
C(15)	−0.309 5(2)	0.338 8(6)	−0.102 6(1)
	−0.309 6(2)	0.338 4(5)	−0.102 7(1)
C(16)	−0.231 3(2)	0.150 0(6)	−0.103 0(1)
	−0.231 0(2)	0.150 3(5)	−0.102 8(1)
H(1)	0.354(2)	0.352(5)	0.312(1)
	0.360(2)	0.348(5)	0.314(1)
H(2)	0.350(2)	0.710(5)	0.399(1)
	0.350(1)	0.711(5)	0.401(1)
H(3)	0.186(2)	0.953(6)	0.352(1)
	0.186(1)	0.961(5)	0.354(1)
H(4)	0.029(2)	0.843(5)	0.225(1)
	0.027(2)	0.846(4)	0.226(1)
H(5)	−0.276(2)	0.816(5)	0.030(1)
	−0.274(2)	0.825(5)	0.034(1)
H(6)	−0.461(2)	0.873(6)	−0.058(2)
	−0.462(2)	0.880(5)	−0.057(1)
H(7)	−0.550(2)	0.590(5)	−0.175(1)
	−0.552(2)	0.591(4)	−0.175(1)
H(8)	−0.456(2)	0.263(6)	−0.204(1)
	−0.457(2)	0.259(5)	−0.204(1)

* Upper and lower values quoted are for Levels I and II structure refinements respectively. Mn is at (0,0,0).

electron contribution to the calculated structure factor. During the refinement, orbital populations were constrained to lie between 0.0 and 2.0 e.

From this valence-electron model, it was apparent that the contribution to all the data from aspherical valence density effects on the C and N atoms was significant. The effects of the aspherical valence density on C and N were then included in the scattering model. A crude but effective way of doing this, using the crystallographic programs at our disposal (' *X*-Ray '76 '),[8] was to include in the scattering model 26 spherical ' blobs ' of charge at the mid-points of the C–C and C–N bonds and on the Mn–N bonds at positions one-third of the bond distance from N. This was done,

TABLE 2 †

Final atomic thermal parameters for [Mn(pc)] at 116 K. Upper and lower values quoted are for Levels I and II structure refinements respectively, U tensors in Å^2. Anisotropic and isotropic thermal parameters are defined by $T = \exp[-2\pi^2(h^2a^{*2}U_{11} + k^2b^{*2}U_{22} + l^2c^{*2}U_{33} + 2hka^*b^*U_{12} + 2hla^*c^*U_{13} + 2klb^*c^*U_{23})]$ and $T = \exp[-8\pi^2U(\sin^2\theta)/\lambda^2]$

Atom	10^3U_{11}	10^3U_{22}	10^3U_{33}	10^3U_{12}	10^3U_{13}	10^3U_{23}
Mn	15.0(3)	19.4(3)	17.2(3)	1.6(3)	8.1(2)	−2.5(3)
	12.5(3)	17.0(3)	14.9(3)	1.8(3)	6.7(2)	−2.5(3)

† The complete Table 2 has been deposited in Supplementary Publication No. SUP 22755.

using the H form factor modified by individual isotropic Gaussian functions, initially chosen with $U = 0.038$ Å^2, as the scattering curves for the spherical overlap charges, and using individual populations initially fixed at 0.2 e. The presence of such bonding charge between the aromatic C–C bonds in benzene rings has been discussed previously,[18] and its neglect leads to incorrect atomic positions as

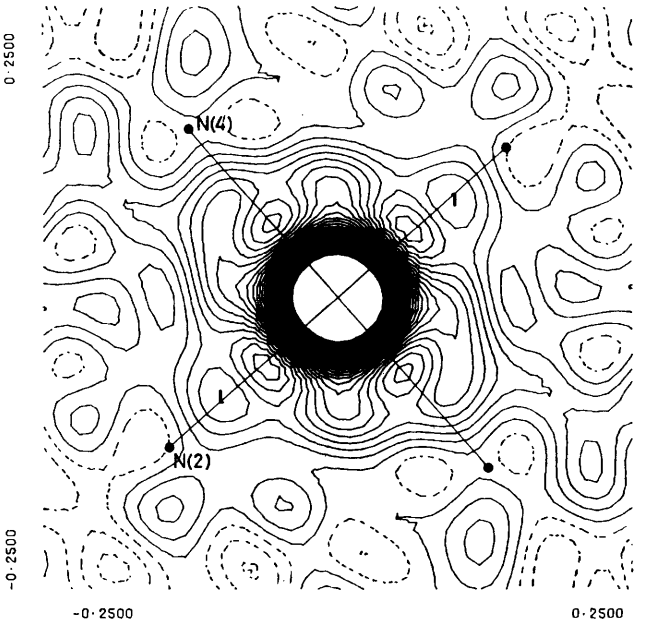

FIGURE 2 Section through the MnN_4 co-ordination plane, showing the valence-electron density in [Mn(pc)]; a difference synthesis using only the Ar core contribution to the Mn scattering. Contour levels as in Figure 1; however, contours are only drawn to *ca.* 3.5 e Å^{-3} and hence the large positive density near the Mn nucleus is not contoured

determined by *X*-ray diffraction analysis.[3,18] The scattering model was refined by least squares, minimising $\Sigma w(\Delta I)^2$, in two blocks using an iterative procedure. In the first cycles, the overall scale, positional, and thermal parameters of C, H, N, and Mn, and the atom population of Mn (220 variables) were refined in one block while the bonding charges were held invariant. During these cycles, the

benzene C atoms moved further out from the centroids of the benzene rings and close to the true nuclear positions.[3] The isotropic Gaussian functions and populations of the individual bonding charges, together with the overall scale factor, were then refined (53 variables) while all other parameters were held invariant. The two refinements were repeated successively until the model converged with $R = 0.045$, $R' = 0.060$, and $\chi = 1.301$ (272 variables). The maximum shift-to-error ratio at convergence was 0.06 : 1. Final atomic positional co-ordinates and thermal parameters from this stage of refinement (Level II) are listed in Tables 1 and 2 and the bonding charge parameters in Table 4. Some difference-Fourier sections (Figure 3), calculated at this stage of the refinement, indicate the extent to which the spherical overlap charges have been able to model the aspherical valence-electron density observable about the C and N atoms in Figure 1. In this Level II refinement the atom population of Mn was allowed to vary, and refined to the value 0.991(2). The refinement of this population, together with the overall scale factor, accounts for variations in the ratios of the C and N charges to the Mn charge on including the overlap charges without changing the populations of the centrosymmetrical components of the C and N atoms from unity. This Mn atom population was used for the difference-Fourier syntheses of Figure 3. However, in the calculations of structure factors below involving only the Ar core of Mn, an atom population of unity was used for Mn. Observed and calculated structure factors are listed in SUP 22755.

TABLE 3

Orbital populations for the Mn atom in [Mn(pc)] [a]

Variables used in refinement	Level I ' difference ' structure factors containing contributions from Mn valence electrons plus residual bonding densities		Level II ' difference ' structure factors containing only Mn valence-electron contributions				
	1 151 reflections [b]	2 023 reflections [c]	1 151 reflections [b]	2 023 reflections [c]	1 356 reflections [d]	2 265 reflections [e]	1 886 reflections
$3d_{xy}$	2.0(5)	1.8(4)	2.0(2)	1.6(2)	1.8(2)	1.5(2)	1.5(2)
$3d_{xz}$	0.4(4)	0.0(3)	0.8(2)	0.6(2)	0.9(2)	0.6(2)	0.6(2)
$3d_{yz}$	0.7(4)	0.2(3)	1.0(2)	0.7(2)	1.0(2)	0.7(2)	0.7(2)
$3d_{z^2}$	0.5(5)	1.2(4)	0.7(3)	1.1(2)	0.5(3)	0.9(2)	0.9(2)
$3d_{x^2-y^2}$	0.0(5)	0.0(4)	0.0(3)	0.2(2)	0.0(3)	0.1(2)	0.1(2)
$4s$	2.0(2)	2.0(2)	1.8(2)	1.9(2)	2.0(3)	2.0(3)	2.0(3)
r_{3d} [g]	0.72(4)	0.71(4)	0.97(4)	0.96(4)	0.92(4)	0.91(4)	0.90(5)
r_{4s} [g]	0.84(6)	0.83(6)	0.92(7)	0.90(7)	0.85(6)	0.83(5)	0.83(6)
χ [h]	1.680	1.520	1.319	1.295	1.331	1.288	1.366

[a] The least-squares derived estimated standard deviations are given in parentheses for each variable. The x–y–z quantisation axes on Mn are defined with x along the Mn–N(2) bond, z perpendicular to the MnN_4 co-ordination plane and y orthogonal to x and z. [b] $(h + l) = 2n$ data; $(\sin\theta)/\lambda \leqslant 0.595$ Å^{-1}. [c] All data within $(\sin\theta)/\lambda \leqslant 0.595$ Å^{-1}. [d] $(h + l) = 2n$ data; $(\sin\theta)/\lambda \leqslant 0.662$ Å^{-1}. [e] All data within $(\sin\theta)/\lambda \leqslant 0.662$ Å^{-1}. [f] All data with $|F_o| > 5.0$ (absolute units). [g] r is the parameter, discussed in the text, associated with variation of the radial exponents of the atomic wave function. [h] The goodness-of-fit index $\chi = [\Sigma w(\Delta F_d)^2/(N - V)]^{\frac{1}{2}}$, where $\Delta F_d (= |F_d - F_v|)$ is the difference between observed and calculated ' difference ' structure factors and N and V are the numbers of observations and variables respectively.

TABLE 4

Final populations (e) and isotropic Gaussian parameters, U (Å^2), for the bonding charges. The scattering curves for the bonding charges were the H scattering curve [12] modified by the function $T = \exp[-8\pi^2 U(\sin^2\theta)/\lambda^2]$

Bonding charge *	Population	10^2U
Mn–N(2)	0.40(8)	9(5)
Mn–N(4)	0.45(8)	10(4)
N(1)–C(1)	0.29(4)	−3(2)
N(1)–C(16')	0.21(4)	−3(2)
N(2)–C(1)	0.06(3)	−7(3)
N(2)–C(8)	0.08(3)	−8(2)
N(3)–C(8)	0.20(3)	−5(2)
N(3)–C(9)	0.19(3)	−5(2)
N(4)–C(9)	0.10(3)	−6(3)
N(4)–C(16)	0.03(2)	−9(6)
C(1)–C(2)	0.14(3)	−6(2)
C(2)–C(3)	0.23(3)	−5(1)
C(2)–C(7)	0.17(3)	−5(2)
C(3)–C(4)	0.26(4)	−2(2)
C(4)–C(5)	0.26(4)	−3(2)
C(5)–C(6)	0.23(3)	−4(2)
C(6)–C(7)	0.24(3)	−5(1)
C(7)–C(8)	0.15(3)	−6(2)
C(9)–C(10)	0.14(3)	−8(2)
C(10)–C(11)	0.25(4)	−2(2)
C(10)–C(15)	0.22(4)	−4(2)
C(11)–C(12)	0.15(3)	−7(1)
C(12)–C(13)	0.29(5)	1(3)
C(13)–C(14)	0.22(4)	−3(2)
C(14)–C(15)	0.19(3)	−6(1)
C(15)–C(16)	0.15(3)	−6(2)

* The spherical bonding charge density was placed in the mid-point of the Level I C–C and C–N bonds, and in the Mn–N bond at a distance one-third of the bond length from the N atom.

A new set of ' difference structure factors ', F_d, was calculated as before, using F_c from the Level II stage of refinement. In this case, the valence electrons of Mn together with experimental errors in the observed data were the major contributors to F_d, and a least-squares refinement of a valence-electron model for Mn, using the program ASRED as before, was reasonably successful. The final orbital populations for Mn from refinements using different portions of the data are presented in Table 3. The $(\sin\theta)/\lambda$ cut-off of 0.595 Å^{-1} was employed in certain refinements as the data were complete to this limit. In the determination of the ' difference structure factors ', there is a possibility, discussed in the Appendix, that F_d will be incorrectly calculated for cases with $|F_c| < |F_d|$ because of the uncertainty in the phase of F_o in these cases. A refinement of the valence-electron model for Mn was also performed on all the data excepting those reflections with $|F_o| < 5.0$ (absolute units), and the results are presented in

Table 3. The values of $|F_d|$ calculated from the valence-electron scattering model were considerably less than 5.0 for most of the data. Thus this latter refinement excluded data for which there was a possibility that F_d was incorrectly calculated, as well as excluding those reflections

TABLE 5

Parameters for the Mn atom in [Mn(pc)] from the simultaneous least-squares refinement of thermal and orbital parameters [a] with estimated standard deviations in parentheses

Variables	Final value
U_{11} [b]	0.011 2(5)
U_{22}	0.016 0(4)
U_{33}	0.012 9(4)
U_{12}	0.001 5(4)
U_{13}	0.005 4(2)
U_{23}	−0.003 9(4)
$3d_{xy}$ [c]	1.8(2)
$3d_{xz}$	0.5(2)
$3d_{yz}$	1.2(2)
$3d_{z^2}$	1.0(2)
$3d_{x^2-y^2}$	0.9(2)
$4s$	0.8(3)
r_{3d} [d]	1.18(6)
r_{4s}	1.2(3)

[a] The goodness-of-fit index χ, as defined in Table 3, was 1.286 for 2 265 observations and 14 variables. [b] U tensors, in Å², are as defined in Table 2. [c] The x–y–z quantisation axes on Mn are as defined in Table 3. [d] r is the parameter, discussed in the text, associated with variation of the radial exponents of the atomic wave function.

in which there were relatively large experimental errors in $|F_o|$ and hence F_d.

The final stage in the refinement of the valence-electron model for Mn included the simultaneous refinement of the anisotropic thermal factor for Mn, with the $3d$ and $4s$ orbital populations. For this purpose, to the Level II F_d values were added the structure factor contributions of the Ar core of Mn^{2+}. The resulting phased structure factors contained the total contribution of the Mn atom to the scattering, with only a very small contribution from any bonding charge density on the macrocyclic ligand not accounted for by the scattering model. The results of this least-squares refinement, using the program ASRED as before, are presented in Table 5.

In the refinements of the valence-electron models for Mn, the $\langle j_0 \rangle$, $\langle j_2 \rangle$, and $\langle j_4 \rangle$ scattering curves for the $3d$ electrons of Mn^{2+} were used,[13] while the $4s$ scattering curve was

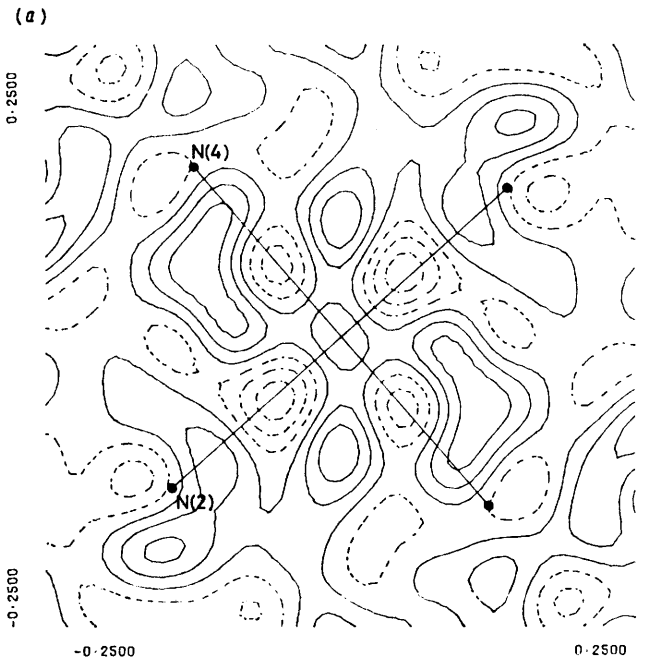

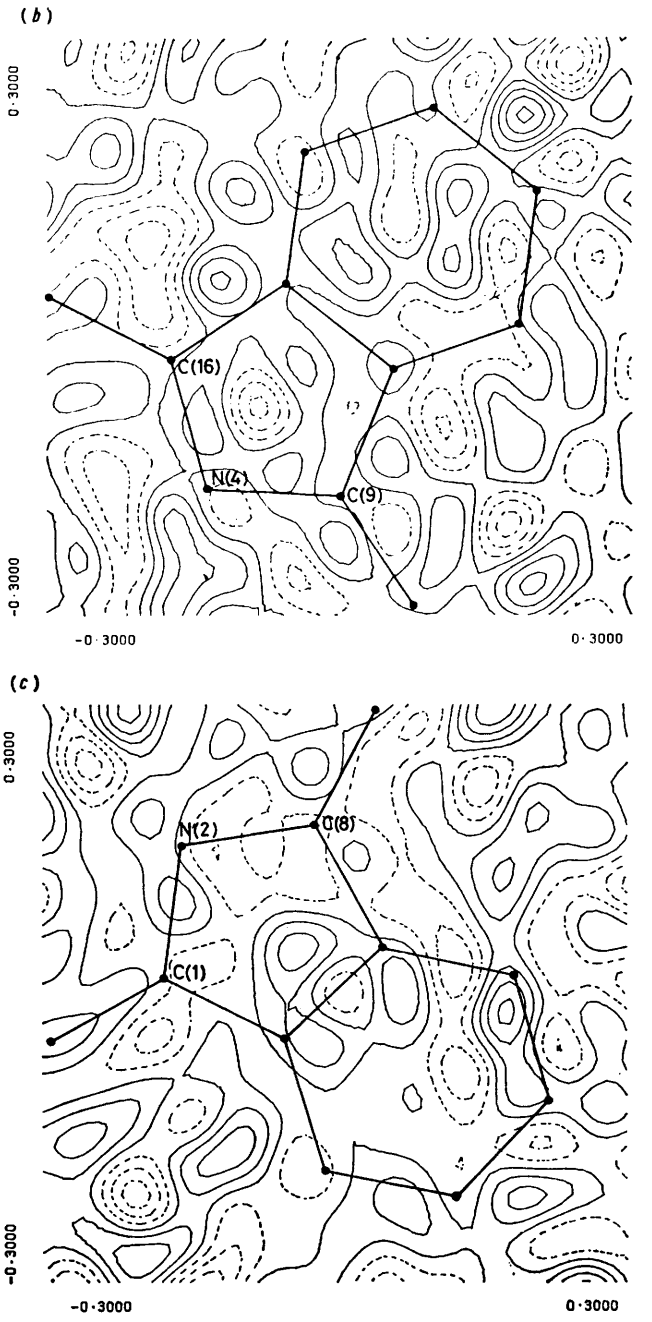

FIGURE 3 Sections of the deformation density in [Mn(pc)], after the Level II stage of refinement in which the bonding density was included as spherical charges in the scattering model. Contours as in Figure 1; dimensions of each section in nm. (*a*) Section through the MnN_4 co-ordination plane, centred on the Mn atom. (*b*) and (*c*) Sections through the pyrrole and benzene residues

calculated [19] from a wave function for Mn^+ with $\zeta = 1.8$.[16] All the computations were performed on a CDC CYBER 73 computer at the Western Australian Regional Computing Centre.

RESULTS OF STRUCTURE REFINEMENTS

The molecular geometry and atom numbering of the centrosymmetric [Mn(pc)] molecule are shown in Figure 4. The manganese atom has essentially D_{4h} symmetry, with angles N(2)–Mn–N(4) and N(2)–Mn–N(4′) of 90.96(8) and 89.04(8)° respectively (Level II refinement values). Interatomic distances (Table 6) and angles (tabulated in SUP 22755) are given for both Levels I and II of refinement. The bond lengths and angles from the present refinements have consistently lower estimated standard deviations than those from the previous refinement,[1] which are also presented in the Tables. This increased accuracy is a result of including all the data (including negative intensities), as distinct from the $3\sigma(I)$ rejection criterion used previously. For Level I the maximum non-hydrogen-atom bond length and angle changes are respectively 1.0 pm and 0.5°, with averages of 0.4 pm and 0.2°. The bond lengths from the Level II refinement differ from those obtained from the conventional refinements in which bonding charge density on the ligand is ignored. In particular, the weighted mean values of the 12 individual benzene ring C–C bond distances from the Level I and II refinements are 139.0(2) and 139.7(1) pm, respectively. As discussed elsewhere,[3,18] the neglect of aspherical valence-charge density in an X-ray diffraction analysis of molecular structure, using data of limited resolution [*e.g.* $(\sin\theta)/\lambda < 0.7$ Å^{-1}], can cause the apparent shortening of bond distances. Because some attempt has been made at the Level II stage of refinement to include the effects of overlap charge density in the C–C, C–N, and Mn–N bonds, the bond distances obtained in this refinement are expected to approach more closely the true internuclear distances obtained from neutron diffraction methods, and a comparison with the results of a 4.2 K neutron diffracton study of [Co(pc)][3] reveal this to be the case.

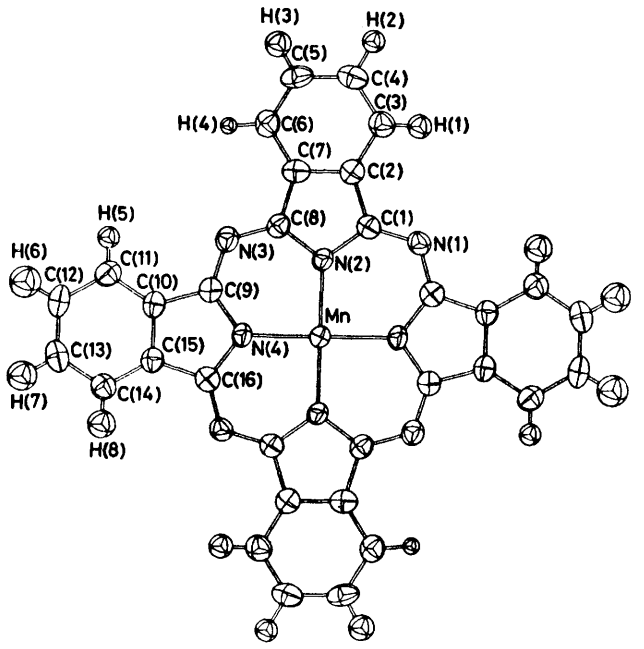

FIGURE 4 An ORTEP drawing of [Mn(pc)] (116 K parameters) showing the molecular geometry and atom numbering. The thermal ellipsoids are drawn at the 80% probability level

Because of the improvements in accuracy and nuclear positions in the Levels I and II atomic parameters, some displacements from and angles between mean planes occur and are deposited in Tables (available in SUP 22755). For each of Levels I and II, relative to the previous refinement, no change in displacement values greater than 0.4 pm, nor in mean plane angle greater than 0.1°, occurs.

DISCUSSION

General Assessment of the Analysis.—Chemically significant 3*d* and 4*s* orbital populations have been obtained (Table 3) for the manganese atom in [Mn(pc)], from our analysis of the 116 K single-crystal X-ray diffraction data of moderate extent [$(\sin\theta)/\lambda \leqslant 0.662$ Å^{-1}]. The results of the orbital population refinements using various sections of data (Table 3) show that the overall trend amongst these populations is not strongly dependent on the portion of the data set used in the refinement. The inclusion of more extensive data in the refinements in each case yielded lower standard deviations in the orbital populations. Our analysis suffers from some obvious limitations introduced by the shortcomings of the data set and the crudity of some features of the scattering model. The fact that it is a model-dependent orbital population analysis is a limitation from some points of view, although we defend it for the discussion of features of chemical interest on the grounds that there are ambiguities in the translation of more rigorous approaches, such as the method of multipole analysis, into chemical terms.

It was apparent during the population analyses that if some account was made in the scattering model for the aspherical valence-electron density about the ligand atoms, the least-squares refinement of the 4*s* and 3*d* orbital populations was well behaved, and the resultant populations had smaller standard deviations than those from refinements in which no account of the ligand valence-electron density was made. In the Level II stage of the present analysis, the ligand valence-electron density was modelled by spherical charges of variable populations and scattering factors, placed at the midpoints of the C–C and C–N bonds. No attempt was made to represent the ' out-of-plane ' nature of the π bonding in the ligand. While the physical limitations of this empirical model are obvious, it is a useful ploy to obtain a better scattering model with a lower goodness of fit than the conventional spherical atom approach, on which to base a refinement of the valence orbital populations on the manganese atom. Also the bond distances obtained from this model, in the benzene rings in particular (Table 6), are closer to those obtained from neutron diffraction [3] than are those values obtained from the conventional refinement neglecting bonding charge density (Level I values, Table 6). For X-ray diffraction data sets of high accuracy and extending to high $(\sin\theta)/\lambda$ values, collected specifically for the purpose of accurate

electron density studies on transition-metal atoms, a more sophisticated level of treatment of ligand valence-electron density may prove advantageous. Rather than spheres, the bonding charge could be represented by ellipsoids to take account of the more extended density perpendicular to the plane of a benzene ring.[18] Alternatively, a multipole refinement of the ligand electron density,[20] or the aspherical atom refinement proposed by Hellner,[21] are possible means of including the ligand valence-electron density in the scattering model.

TABLE 6

Interatomic distances (Å) in [Mn(pc)] at 116 K

	Previous $3\sigma(I)$ refinement	Level I refinement	Level II refinement
(*a*) Intramolecular distances *			
Mn–N(2)	1.939(3)	1.936(2)	1.940(2)
Mn–N(4)	1.942(3)	1.940(2)	1.944(2)
N(1)–C(1)	1.325(5)	1.319(4)	1.329(3)
N(1)–C(16′)	1.316(4)	1.314(4)	1.319(3)
N(2)–C(1)	1.396(3)	1.402(3)	1.394(2)
N(2)–C(8)	1.380(5)	1.383(4)	1.381(3)
N(3)–C(8)	1.326(4)	1.327(3)	1.331(3)
N(3)–C(9)	1.321(4)	1.328(3)	1.329(2)
N(4)–C(9)	1.379(5)	1.381(4)	1.381(3)
N(4)–C(16)	1.392(3)	1.399(3)	1.391(2)
C(1)–C(2)	1.450(5)	1.451(4)	1.449(3)
C(2)–C(3)	1.399(4)	1.398(3)	1.403(3)
C(2)–C(7)	1.393(5)	1.394(4)	1.396(3)
C(3)–C(4)	1.384(6)	1.377(5)	1.391(4)
C(4)–C(5)	1.393(5)	1.393(4)	1.403(4)
C(5)–C(6)	1.385(4)	1.381(3)	1.392(3)
C(6)–C(7)	1.396(6)	1.393(4)	1.401(4)
C(7)–C(8)	1.444(4)	1.443(3)	1.441(3)
C(9)–C(10)	1.451(4)	1.446(3)	1.445(3)
C(10)–C(11)	1.395(6)	1.385(5)	1.397(4)
C(10)–C(15)	1.391(4)	1.395(3)	1.398(3)
C(11)–C(12)	1.386(4)	1.390(4)	1.396(3)
C(12)–C(13)	1.391(5)	1.387(4)	1.400(4)
C(13)–C(14)	1.388(6)	1.382(5)	1.393(4)
C(14)–C(15)	1.397(4)	1.394(3)	1.399(3)
C(15)–C(16)	1.453(5)	1.453(4)	1.453(4)
H(1)–C(3)	0.95(4)	0.95(3)	1.00(2)
H(2)–C(4)	1.02(3)	1.03(2)	1.04(2)
H(3)–C(5)	0.96(5)	0.96(3)	0.99(3)
H(4)–C(6)	0.92(4)	0.97(2)	0.99(2)
H(5)–C(11)	0.93(3)	0.92(2)	0.97(2)
H(6)–C(12)	0.97(5)	0.98(3)	1.02(3)
H(7)–C(13)	0.98(4)	1.00(2)	1.00(2)
H(8)–C(14)	0.93(4)	0.94(2)	0.95(2)
Mn · · · N(1)	3.400(2)	3.399(2)	3.407(2)
Mn · · · N(3)	3.356(3)	3.358(3)	3.364(2)
N(2) · · · N(4)	2.765(3)	2.761(2)	2.769(2)
N(2) · · · N(4′)	2.724(4)	2.721(3)	2.723(3)
(*b*) Selected intermolecular contacts perpendicular to molecular plane			
Mn · · · N(3″)	3.150(3)	3.148(3)	3.148(2)
Mn · · · C(8″)	3.410(3)	3.409(3)	3.409(2)
Mn · · · C(9″)	3.546(4)	3.545(3)	3.543(2)

* Primed and double-primed atoms are related to the unprimed atom by the operations $(-x, -y, -z)$ and $(x, -1 + y, z)$ respectively.

In the present analysis, perhaps the most significant error arises from the correlation between the anisotropic thermal motion of the manganese atom and its aspherical valence charge density. In order to obtain the orbital populations in Table 3, anisotropic root-mean-square displacements for the manganese atom were obtained from the least-squares refinement of the structural parameters. The thermal vibration parameters obtained in this way are not correlated with the valence charge asphericity to the same extent as they are for the first-row elements, due to the dominance of the transition-metal core. However, the parameters describing the anisotropy in the electron density about the manganese atom due to thermal motion will also model to some extent the anisotropy of the aspherical valence charge density. The information available for analysis in terms of the manganese atom valence-electron density is, then, the way in which the observed electron density differs from that which can be described by a spherically symmetrical manganese atom subject to anisotropic vibrations. The present experiment succeeds partly because the low temperature involved (116 K) considerably reduces the thermal motion contribution to the asphericity of the charge density on the manganese atom. Probably, it also succeeds partly because the lower site symmetry of the metal atom environment (square planar) leads to higher anisotropy of the valence-electron distribution. It is generally accepted that analysis in terms of valence-electron distributions requires that the thermal motion be accurately accounted for and in principle, the thermal effects should be determined independently or refined simultaneously with the orbital population parameters. However, our attempts at such a simultaneous refinement were unsatisfactory. From the results of this refinement (Table 5), which was very slow to converge, the high degree of correlation between the anisotropic thermal motion and the asphericity due to valence charge density is apparent. The orbital populations are somewhat different from those presented in Table 3, and in particular the $3d_{x^2-y^2}$ orbital has gained significant population at the expense of the $3d_{xz}$ and 4*s* orbitals, and the scattering curves for the 3*d* and 4*s* electrons have changed significantly from the free-atom values, as seen in the ' orbital-expansion ' parameters r, which differ significantly from unity. The results from this simultaneous refinement of thermal motion and valence charge density are not as chemically reasonable as the results presented in Table 3 {in particular, the $3d_{x^2-y^2}$ orbital is generally considered to have zero population in square-planar compounds such as [Mn(pc)]}.[22] It is considered that in the present case such a simultaneous refinement is of little value as the correlation between thermal and valence charge density asphericity causes a significant contribution of the thermal effects into the orbital populations and *vice versa*, and it is not possible to disentangle the two effects. However, such correlation could be minimised significantly by including in the observed data set the reflections to very high $(\sin\theta)/\lambda$ values, to which the contributions of the valence electrons on the metal atom are relatively very small. Alternatively, the thermal motion of the metal atom could be determined independently from a high-angle data refinement, or from neutron diffraction data obtained at the same temperature as the *X*-ray data. In the latter procedure, the neutron diffraction analysis gives nuclear positions, and the amplitudes of vibration, of the atomic nuclei directly and of the electron density

within the context of the Born–Oppenheimer approximation.

Chemical Implications.—It is of considerable interest to compare the 4*s* and 3*d* orbital populations of the manganese ion deduced in this work with bonding to, and the physical properties of, the ion. However, the level at which this may be done is not high, firstly because our simple modelling of the system begs important questions which arise in the quantum mechanical treatment of bonding and secondly, because the theory for a molecule as large as [Mn(pc)] is necessarily crude. Our analysis of within the framework of crystal-field theory or of the angular overlap model, does not yield an ordering of the *d* orbitals likely to lead to an $S = 1$ rather than high spin ($S = 2$) or low spin ($S = 0$) ground term for any reasonable values of the parameters. We have investigated the application of the ligand-field model to [Mn(pc)]. We find that while, as has been demonstrated,[25-28] it is possible to obtain the $S = \frac{3}{2}$ ground term from certain combinations of the ligand-field parameters *Dq*, *Ds*, and *Dt*, or their equivalents, when analysed in terms of, say, angular overlap model para-

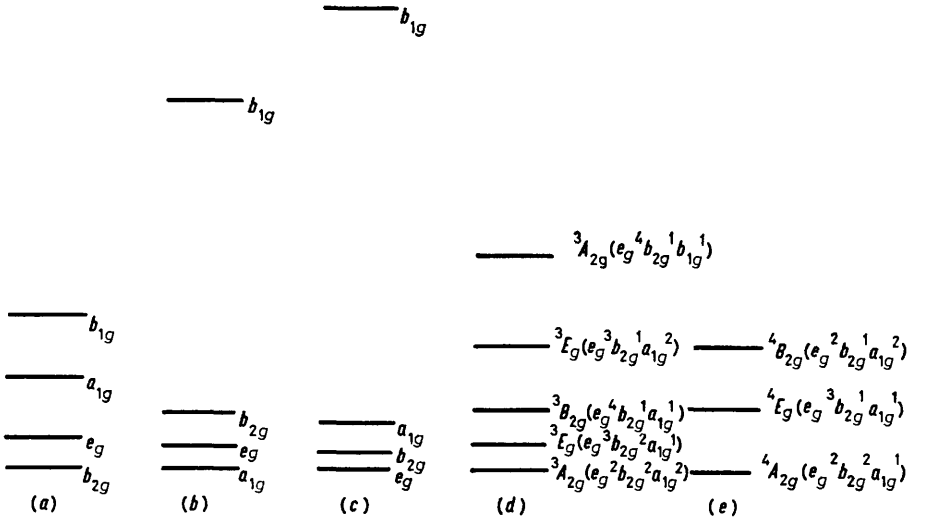

FIGURE 5 *d*-Orbital and term energy ordering sequences for first transition series ions in square-planar stereochemistry such as a phthalocyanine. (*a*) *d*-Orbital sequence arising from four pyridine molecules, based on the angular overlap model with $e_{\pi\perp} = 0.5e_\sigma$. (*b*) *d*-Orbital sequence calculated for [Co(porphyrin)].[24] (*c*) *d*-Orbital sequence calculated for [Fe(pc)].[23] (*d*) Term energy sequence and orbital configurations arising from d^6 occupancy of part (*c*) under interelectronic repulsion perturbation. (*e*) Probable term energy sequence and orbital configurations arising from d^5 occupancy of part (*c*) under interelectronic repulsion perturbation (schematic only)

orbital populations gives the charge on the manganese atom as close to Mn^+, but this figure does not include any contribution from the bonding charges in the Mn–N bonds, near the nitrogen atoms, which must contain some small overlap population contribution from those bonds. A molecular-orbital calculation on [Mn(pc)] itself is not available in the literature to our knowledge, and the most pertinent results are an INDO calculation [23] for crude models of [Fe(pc)] and [Co(pc)] and an *ab initio* calculation [24] of [Co(porphyrin)]. The limitations of the INDO level of calculation, and the limited basis set possible for the *ab initio* calculation of such a large molecule, restrict the conclusions which may be drawn from them to a very qualitative level. For example, in spite of the inclusion of some configurational interaction, the *ab initio* calculation for [Co(porphyrin)] fails to reduce the energy of any doublet term below the lowest quartet, so that the observed low-spin ground term is not reproduced.

The INDO calculation on [Fe(pc)] is probably the more pertinent and relevant for our purposes. Like [Mn(pc)], [Fe(pc)] is an intermediate spin case. It is pointed out [23] that a ligand-field type treatment, whether meters e_σ, $e_{\pi\parallel}$, and $e_{\pi\perp}$, these are not reasonable in the light of their values known for other nitrogen-atom donor systems. If, for example, the angular overlap model parameters for four pyridine molecules are used to calculate a *d*-orbital ordering, such as that illustrated in Figure 5(*a*), no quartet term is very near the ground term. The INDO calculation on [Fe(pc)] and [Co(pc)] suggests that the e_g (d_{xz}, d_{yz}) orbitals lie lowest [see Figure 5(*c*)] followed by the b_{2g} (d_{xy}) orbital, and that the a_{1g} (d_{z^2}) orbital is lowered in energy towards them because it is mixed with the ligand orbitals and with the 4*s* orbital more than are the other *d* orbitals (' differential covalency ' in the parlance of ref. 23). This view is supported by observations of the spectra and magnetic properties of various iron, cobalt, and copper square-planar complexes.[29]

The *ab initio* calculation on [Co(porphyrin)] gives the ordering of the *d* orbitals ($a_{1g} < e_g < b_{2g} \ll b_{1g}$) [Figure 5(*b*)] and shows a much lower relative energy for the a_{1g} orbital than crystal-field predictions, but this orbital does not seem to include much contribution from mixing with the 4*s* metal orbital. This calculation assigns a charge of *ca.* +1.8 e to the cobalt atom from the effective

ionisation of most of the two 4*s* electrons, and *ca.* −0.57 e to each ligand nitrogen atom.

The magnetic susceptibility and anisotropy [30,31] of [Mn(pc)] show that the ground term corresponds to the intermediate spin case $S = \frac{3}{2}$, with no orbital degeneracy and that the ground term is $^4A_{2g}$ or $^4B_{2g}$ rather than ^4E_g. It can be argued that this requires a *d*-orbital sequence $a_{1g} < e_g < b_{2g} \ll b_{1g}$ [Figure 5(*b*)] or $b_{2g} < e_g < a_{1g} \ll b_{1g}$ [Figure 5(*a*)]. However, this is not necessarily so. As discussed in ref. 23 in connection with [Fe(pc)], d^6, and implicit in other calculations [25-28] an order of the type $e_g < b_{2g} < a_{1g} \ll b_{1g}$ can give rise to the configuration $e_g^{2}{\cdot}b_{2g}^{2}{\cdot}a_{1g}^{2}$ with the $^3A_{2g}$ term lowest, rather than the most obvious $e_g^{4}{\cdot}b_{2g}^{1}{\cdot}a_{1g}^{1}$ configuration [see Figure 5(*d*)]. From all the evidence and calculations (except those on a purely ligand-field basis), the e_g-b_{2g}-a_{1g} orbital set seems to be closely spaced in energy for the square-planar phthalocyanine-type compounds of metals from manganese to copper. The point is, that being so, the ground term is not determined primarily by the order within the orbital set, but rather by the effects of inter-electronic repulsions. Accordingly, a $^4A_{2g}$ ground term, say, for [Mn(pc)] may arise from the configuration $e_g^{2}{\cdot}b_{2g}^{2}{\cdot}a_{1g}^{1}$.

The INDO calculation on [Fe(pc)] states that the e_g, b_{2g}, and a_{1g} wave functions have *d*-orbital coefficients of 0.98, 0.97, and 0.82 respectively. There is no statement about the involvement of the 4*s* metal orbital in the bonding nor of effective charge on the iron atom. The *ab initio* calculation on [Co(porphyrin)] gives information about the composition of the lowest terms which arise, and it is stated that there is very little mixing of ligand orbitals with the half-filled metal *d*-orbital, which is a_{1g} (d_{z^2}) for the $^2A_{1g}$ term case. In this calculation the 4*s* electrons are largely lost to the ligand, giving a charge of $Co^{1.8+}$. Our results do not fit in well with all facets of these calculations: we find that the charge on the manganese atom is *ca.* 1+, achieved by the delocalisation of a 3*d* electron (Table 3) rather than the loss of two 4*s* electrons. We must then propose that there is rather extensive mixing of at least some of the *d* orbitals with ligand orbitals; to the extent of *ca.* 24% in fact, from the valence model refinement (Table 3) using all 2 265 observations. Concomitantly, we expect that there should be substantial spin density located on the ligand, and we have observed just that phenomenon in a separate experiment using the technique of polarised neutron diffraction. While that experiment has not yet been fully analysed, we have suggested that *ca.* 20% of the spin of the complex is located away from the manganese atom.[4] The result is in keeping with the ' differential covalence ' explanation for the relative lowering of the energy of the a_{1g} orbital outlined in the INDO calculation, but is much larger in magnitude than that calculation would lead one to expect.

The extensive delocalisation of the *d* orbitals would severely affect arguments about the ordering of the *d* orbitals based upon the magnetic susceptibility or e.s.r. data, since they depend upon the amount of orbital angular momentum associated with each orbital type, and this is likely to be quite sensitive to the admixture of ligand orbitals. The delocalisation could affect the total spin of the system consequent upon changes of the *d*-orbital energies and reduction of interelectronic repulsion parameters and may in part be responsible for the fact that the ground state of [Mn(pc)] is a spin quartet, $S = \frac{3}{2}$.

Given the delocalisation of 24% of the *d*-electron population, the remaining 3.8 *d* electrons located on the manganese atom are distributed amongst the valence molecular orbitals much as expected. If the orbital ordering is accepted to be the same as indicated above [Figure 5(*c*)], for the similar square-planar compounds of iron and cobalt, and that the interelectronic repulsions lead to the configuration $e_g^{2}{\cdot}b_{2g}^{2}{\cdot}a_{1g}^{1}$, the *d*-orbital populations expected if each is equally delocalised are listed in Table 7. It is seen that they compare very favourably with our experimental results.

TABLE 7

Molecular-orbital and *d*-orbital populations predicted for the configuration $e_g^{2}{\cdot}b_{2g}^{2}{\cdot}a_{1g}^{1}$ with 24% *d*-electron delocalisation, compared with deductions from the present work

		d-Orbital occupancy	
Valence molecular orbital	Total occupancy	Predicted assuming 24% delocalisation	Deduced from the present work (Table 3)
b_{1g}	0	0.0	0.1
a_{1g}	1	0.8	0.9
b_{2g}	2	1.5	1.5
e_g	2	1.5	1.3

Our results indicate that the radial extents of the 3*d* and 4*s* manganese orbitals are contracted from the theoretical free-atom values. Our procedure employed as starting premises the form factors of Mn^{2+} for the 3*d* orbitals and of Mn^{+} for the 4*s* orbital. The parameters r_{3d} and r_{4s} of Table 3 are the inverses of linear scalings of the form factors and, being less than unity, indicate that more contracted orbitals are required to account for the data.

APPENDIX

The Derivation of ' Difference Structure Factors ' containing the Transition-metal Valence-electron Contribution to the Scattering in the Centrosymmetric Case.—The anomalous-dispersion-free ' difference structure factor ', F_d, containing the transition-metal valence-electron contribution to the scattering, is obtained from $F_d = F_o - F_c$, where F_o and F_c are phased, dispersion-free observed and calculated structure factors, with only the spherically symmetrical core of the transition metal, together with all other scattering centres, included in the calculation of F_c. The real and imaginary anomalous dispersion contributions, ${}_dA_c$ and ${}_dB_c$, are used to obtain a dispersion-free F_o [32] in the centro-

$$F_o = ({}_dF_o^2 - {}_dB_c^2)^{\frac{1}{2}} - {}_dA_c$$

symmetric case, where $|{}_dF_o|$ is the usual observed structure factor containing a dispersion contribution. The problem

of which argument of $({}_{d}F_{o}^{2} - {}_{d}B_{c}^{2})^{\frac{1}{2}}$ is appropriate is, in general, solved by assuming that F_o and F_c have the same phase. This is so for $|F_c| > |F_d|$. However, when the valence-electron contribution to the scattering is dominant ($|F_d| > |F_c|$), the phase of F_o and hence the sign of the appropriate argument of $({}_{d}F_{o}^{2} - {}_{d}B_{c}^{2})^{\frac{1}{2}}$, is the same as the phase of F_d. After an initial refinement of the valence-electron model using all F_d values derived assuming $|F_c| > |F_d|$, the *calculated* values of the ' difference structure factors ' from the preliminary model were examined in relation with the F_d, F_c, and F_o values, and 13 reflections were found for which the assumption that F_o and F_c have the same phase was obviously incorrect. The F_d values for these cases were correctly determined, using the argument of $({}_{d}F_{o}^{2} - {}_{d}B_{c}^{2})^{\frac{1}{2}}$ of opposite sign to the phase of F_c, and included in subsequent refinements.

If $|({}_{d}F_{o}^{2} - {}_{d}B_{c}^{2})^{\frac{1}{2}}| < |{}_{d}A_{c}|$, the sign of the argument $|({}_{d}F_{o}^{2} - {}_{d}B_{c}^{2})^{\frac{1}{2}}|$ is indeterminate, but any errors arising from the assignment of the phase of F_c to the argument would probably be insignificant in the least-squares refinement method, especially considering that this case only arises for the weakest reflections where there are large experimental uncertainties in $|{}_{d}F_{o}|$. No examples of this type were present, except for a few cases where, due to experimental error, $({}_{d}F_{o}^{2} - {}_{d}B_{c}^{2}) < 0$; the best approximation here is to set ${}_{d}F_{o}^{2} - {}_{d}B_{c}^{2} = 0$. The refinement (Table 3) excluding all examples of this type, as well as all observations with $|F_o| < 5.0$ (absolute units), yielded identical orbital populations to the refinement including all data.

G. A. W. thanks the Australian Institute of Nuclear Science and Engineering for a Research Fellowship. E. S. K. acknowledges receipt of a Commonwealth Postgraduate Research Award. We are grateful to Drs. E. N. Maslen and P. A. Reynolds for stimulating discussions.

[9/1228 *Received*, 3rd *August*, 1979

REFERENCES

[1] R. Mason, G. A. Williams, and P. E. Fielding, *J.C.S. Dalton*, 1979, 676.
[2] B. N. Figgis, R. Mason, and G. A. Williams, *Acta Cryst.*, 1978, **A34**, S158.
[3] G. A. Williams, B. N. Figgis, R. Mason, S. A. Mason, and P. E. Fielding, *J.C.S. Dalton*, 1980, 1688.
[4] B. N. Figgis, R. Mason, A. R. P. Smith, and G. A. Williams, *J. Amer. Chem. Soc.*, 1979, **101**, 3673.
[5] M. Iwata and Y. Saito, *Acta Cryst.*, 1973, **B29**, 822; Y. Wang and P. Coppens, *Inorg. Chem.*, 1976, **15**, 1122; B. Rees and A. Mitschler, *J. Amer. Chem. Soc.*, 1976, **98**, 7918; M. Iwata, *Acta Cryst.*, 1977, **B33**, 59; A. Mitschler, B. Rees, and M. S. Lehmann, *J. Amer. Chem. Soc.*, 1978, **100**, 3390; K. Toriumi, M. Ozima, M. Akaogi, and Y. Saito, *Acta Cryst.*, 1978, **B34**, 1093; K. Toriumi and Y. Saito, *ibid.*, p. 3149; S. Ohba, K. Toriumi, S. Sato, and Y. Saito, *ibid.*, p. 3535; J. N. Varghese and E. N. Maslen, personal communication; R. Goddard and C. Krüger, personal communication.
[6] P. Coppens, in ' Neutron Diffraction,' ed. H. Dachs, Springer–Verlag, Berlin, 1978, p. 71.
[7] ' International Tables for *X*-Ray Crystallography,' Kynoch Press, Birmingham, 1962, vol. 3, p. 162.
[8] J. M. Stewart, ' The *X*-Ray System,' Version of March 1976, Technical Report TR–446, the Computer Science Centre, University of Maryland.
[9] F. L. Hirshfeld and D. Rabinovich, *Acta Cryst.*, 1973, **A29**, 510.
[10] D. T. Cromer and J. B. Mann, *Acta Cryst.*, 1968, **A24**, 321.
[11] D. T. Cromer and D. Liberman, *J. Chem. Phys.*, 1970, **53**, 1891.
[12] R. F. Stewart, E. R. Davidson, and W. T. Simpson, *J. Chem. Phys.*, 1965, **42**, 3175.
[13] ' International Tables for *X*-Ray Crystallography,' Kynoch Press, Birmingham, 1974, vol. 4, pp. 103—146.
[14] R. J. Weiss and A. J. Freeman, *J. Phys. Chem. Solids*, 1959, **10**, 147.
[15] R. E. Watson and A. J. Freeman, *Acta Cryst.*, 1961, **14**, 27.
[16] E. Clementi and C. Roetti, *Atomic Data and Nuclear Data Tables*, 1974, **14**, 177.
[17] R. McWeeney, *Acta Cryst.*, 1951, **4**, 513; B. Dawson, *ibid.*, 1964, **17**, 990, 997.
[18] A. M. O'Connell, A. I. M. Rae, and E. N. Maslen, *Acta Cryst.*, 1966, **21**, 208.
[19] J. Avery and K. J. Watson, *Acta Cryst.*, 1977, **A33**, 679.
[20] N. K. Hansen and P. Coppens, *Acta Cryst.*, 1978, **A34**, 909.
[21] E. Hellner, *Acta Cryst.*, 1977, **B33**, 3813; D. Mullen and E. Hellner, *ibid.*, 1978, **B34**, 2789.
[22] S. F. A. Kettle, ' Co-ordination Compounds,' Nelson, London, 1969.
[23] D. W. Clack and M. Monshi, *Inorg. Chim. Acta*, 1977, **22**, 261.
[24] H. Kashiwagi, T. Takada, S. Obara, E. Miyoshi, and K. Ohno, *Internat. J. Quantum Chem.*, 1978, **14**, 13.
[25] E. König and R. Schnakig, *Inorg. Chim. Acta*, 1973, **7**, 383.
[26] E. König and R. Schnakig, *Theor. Chim. Acta*, 1973, **30**, 205.
[27] G. M. Harris, *Theor. Chim. Acta*, 1968, **10**, 119.
[28] E. König and S. Kremer, ' Ligand Field Energy Diagrams,' Plenum Press, New York, 1977.
[29] R. J. Ford and M. A. Hitchman, *Inorg. Chim. Acta*, 1979, **33**, L167, and refs. therein.
[30] C. G. Barraclough, R. L. Martin, S. Mitra, and R. C. Sherwood, *J. Chem. Phys.*, 1970, **53**, 1638.
[31] C. G. Barraclough, A. K. Gregson, and S. Mitra, *J. Chem. Phys.*, 1974, **60**, 962.
[32] E. J. Gabe, in ' Crystallographic Computing Techniques,' ed. F. R. Ahmed, Munksgaard, Copenhagen, 1975, p. 473.